UNIVERSITY^OF BIRMINGHAM

Research at Birmingham

Microstructure and mechanical behaviour of a Mg94Zn2Y4 alloy processed by equal channel angular pressing

Wu, Jing; Shi, Q.; Ma, H.C.; Chiu, Yu-Lung

Link to publication on Research at Birmingham portal

Author's Accepted Manuscript

Microstructure and mechanical behaviour of a $Mg_{94}Zn_2Y_4$ alloy processed by equal channel angular pressing

J. Wu, Q. Shi, H.C. Ma, Y.L. Chiu
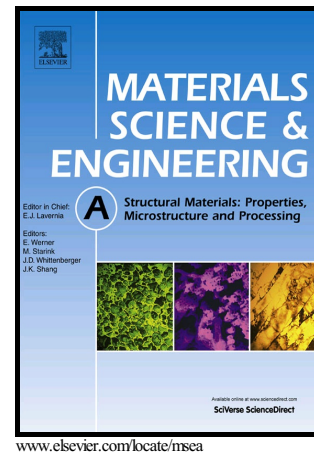
Cite this article as: J. Wu, Q. Shi, H.C. Ma and Y.L. Chiu, Microstructure and mechanical behaviour of a $Mg_{94}Zn_2Y_4$ alloy processed by equal channel angula pressing, *Materials Science & Engineering A* http://dx.doi.org/10.1016/j.msea.2016.05.107

Microstructure and mechanical behaviour of a $Mg_{94}Zn_2Y_4$ alloy processed by equal channel angular pressing

J. Wu[1*], Q. Shi[2], H.C. Ma[1], Y.L. Chiu[1]

[1] School of Metallurgy and Materials, University of Birmingham, Edgbaston, Birmingham, B15 2TT, UK

[2] Department of Materials, Loughborough University, LE11 3TU, UK

Abstract

A $Mg_{94}Zn_2Y_4$ (at.%) alloy containing the long-period stacking ordered (LPSO) phase and the $Mg_{24}Y_5$ phase was processed by equal channel angular pressing (ECAP). The ECAP processing develops a bimodal microstructure consisting of large deformed grains (Mg and LPSO) and sub-micron sized dynamically recrystallised (DRXed) grains. The DRXed grain boundaries are decorated with a large numbers of nano-sized $Mg_{24}Y_5$ precipitates. The presence of LPSO lamellae refined the deformed grains by kinking and promoted dynamic recrystallization during the ECAP process. The ECAP processed alloy was then subjected to the small punch test (SPT). SPT result shows that the ECAP processing increased significantly the strength of the alloy. Under the biaxial tensile stress induced by SPT, the sample started to crack along the ECAP shear direction shortly after the linear elastic region on the load-displacement curve, and the DRXed grains are potential crack sources. These phenomena may be explained by different deformation behaviours of the fibre textured coarse grains and the random oriented DRXed grains, and the distribution of the DRXed grains.

Key words: Mg-Zn-Y alloy; Bimodal structure; ECAP; LPSO phase; Small punch test (SPT); Fracture.

1. Introduction

---

* Corresponding author. Tel. +44 7549644941. Email address: jxw256@bham.ac.uk (Jing Wu)

High strength and ductility are always desirable for structural alloys. This is also true for magnesium based alloys for structural applications. Recently, a Mg-Zn-Y alloy containing a long-period stacking ordered (LPSO) phase has been heavily researched due to its excellent mechanical properties at room temperature and elevated temperatures [1-3]. Much of the work has focused on its structure, strengthening effect, thermal stability and deformation behaviour [4-9]. Thermo-mechanical processes, e.g. hot extrusion, hot rolling and equal channel angular pressing (ECAP), have been carried out on the as-cast alloy to further improve its mechanical performance [10-12]. These thermo-mechanical processes of magnesium alloys often result in the bimodal microstructure, containing coarse grains (including deformed Mg grains and bulk LPSO phases) and fine dynamically recrystallised (DRXed) Mg grains [10, 12,13].

Yamasaki et al. [10] studied as-extruded $Mg_{97}Zn_1Y_2$ alloys and suggested that the small, random orientated DRXed grains increased the ductility, while the textured, coarse grains contribute to the strength. Their results [10] were based on the uniaxial tensile/compression tests performed in the direction of extrusion. Since the bimodal structure shows distinct differences along the extrusion and transverse directions of the processed sample, it is interesting and important to study the deformation and cracking behaviour and when other directions are involved in the deformation.

Small punch test (SPT) is a disc bending technique, which was originally designed for testing radiated samples with limited size in the nuclear power industry. It can also be used to analyse the elastic-plastic properties, the ductile fracture toughness J_{IC} and the brittle fracture toughness K_{IC} [14, 15]. SPT involves applying a force with a spherical indenter to a thin round disc with the edge clamped by a fixture, as shown in Figure 1a. The displacement of the indenter and the force are recorded [16]. As the stress on the disk caused by the spherical indenter is symmetrical along radial directions, it provides a good method to compare the mechanical behaviour and fracture of the bimodal structure in all directions.

In the present study, ECAP is used to modify the as-cast $Mg_{94}Zn_2Y_4$ alloy with the aim of obtaining the bimodal structure and improving the mechanical properties. The mechanical behaviour and fracture of the bimodal structure will be investigated by SPT. The role of coarse grains and DRXed grains in the fracture will be discussed.

2. Experimental

$Mg_{94}Zn_2Y_4$ alloys were prepared in an induction furnace under an argon atmosphere using commercially pure magnesium, pure zinc and an Mg-30 wt.% Y master alloy. Specimens of 10 mm (width) × 10 mm (height) × 20 mm (length) were cut from the as-cast ingot using a CUT 20 High Precision Wire cut EDM machine. The specimens were ECAP processed for 1, 2 and 3 passes at 300 °C with back pressure. The channel angle Φ and the outer arc angle Ψ of the ECAP die are 90° and 36°, respectively. The specimens were rotated 90 degrees along the same direction between two consecutive passes. The forward pressure and backward pressure during the ECAP were maintained at about 700 MPa and 50 MPa, respectively. After the ECAP process, the three orthogonal planes x, y and z of the sample are defined as perpendicular to the extrusion direction (ED), the transverse direction (TD) and the longitudinal direction (LD) respectively after ref [17].

SPT was performed on disc-shaped specimens of Φ8×0.5 mm. Thin discs of the ECAPed samples were sectioned parallel to the y plane. The diameters of the loading ball and the lower die for the SPT were 2.4 mm and 4.5 mm respectively. A constant displacement rate of 0.1 mm/min was imposed during the SPTs and the tests were stopped when a 20 % load drop was reached. Three tests were carried out under each condition.

The microstructures of the specimens were characterised using optical microscope (OM, ZEISS Axioskop 2), scanning electron microscope (SEM, TESCAN MIRA-3 with an Oxford X-Max SDD detector), and transmission electron microscope (TEM, JEOL 2100 with Oxford Instruments Si(Li) Detector). The deformed microstructures were also characterised using conventional electron back-scattered diffraction

(EBSD) and SEM Transmission Kikuchi Diffraction (TKD, also referred as transmission EBSD [18]) on thin foil samples. The spatial resolution of TKD is typically below 10 nm [18]. The specimens of the ECAPed samples for microstructural characterisation were sectioned close to the central region and parallel to the y plane. The samples for OM observation were etched in a solution containing 4 ml nitric acid and 96 ml ethanol. Samples for TEM observation were cut from the bulk using the EDM machine, ground mechanically down to 150 μm and then twin-jet polished using a solution containing 8.8 g lithium chloride, 19.3 g magnesium perchlorate, 833 ml methanol and 167 ml butoxyethanol at -30 °C and 70 V.

3. Results

3.1 The microstructure of the $Mg_{94}Zn_2Y_4$ alloy before and after ECAP processing

Figure 2a shows a typical SEM backscattered electron image obtained from the as-cast $Mg_{94}Zn_2Y_4$ alloy. The matrix in dark contrast is α-Mg. The secondary phases located along the grain boundaries or between the dendritic arms were identified using TEM bright field imaging and selected area diffraction patterns (Figure 2 b-d). The lamellar shaped phase in Figure 2a contains the LPSO phase, which corresponds to the black phase in the TEM image. Figure 2c shows that the diffraction pattern obtained from the LPSO phase is consistent with rhombohedral 18R type structure (R3m, a = 0.322 nm, c = 4.69 nm) [19]. The LPSO phase has a specific orientation relationship with the magnesium matrix, i.e. $(0001)_{LPSO}//(0001)_{Mg}$, $[1210]_{LPSO}//[1210]_{Mg}$ [19, 20], consistent with the observation that the LPSO phases lie in the same direction throughout the one grain (Figure 2a).The phase showing brighter contrast than the LPSO phase in the SEM image (Figure 2a) was identified as $Mg_{24}Y_5$. $Mg_{24}Y_5$ was usually found to be attached to the LPSO phase or between two LPSO lamellae forming a sandwich configuration. The diffraction pattern in Figure 2d was obtained along the [111] zone axis of the $Mg_{24}Y_5$ phase.

Figure 3 shows the microstructures obtained from a transverse section (y plane) of the $Mg_{94}Zn_2Y_4$ alloy after different numbers of ECAP passes. The ED and the LD are indicated by the arrows. In contrast to the as-cast condition (Figure 3a), it can be seen that after 1-pass ECAP (Figure 3b) the grains are

4

elongated and obvious flow lines can be observed. However, no obvious refining of the grains or of the LPSO phase was observed. The LPSO phase in the 1-pass sample tends to lie in the direction inclined to the shear direction (45° from ED towards LD). Some black regions, which were identified as $Mg_{24}Y_5$ particles and DRXed Mg grains, can be observed along grain boundaries and large LPSO phase boundaries. After 2 ECAP passes, the Mg grains were further fragmented, and the fraction of the DRXed Mg region increased. This trend continued in the 3 ECAP passes sample. The microstructure after 3 ECAP passes remained heterogeneous.

The 2-pass ECAPed sample was analysed using SEM for better imaging of the DRXed grains (the dark area in Figure 3c). Figure 4a and 4b show the backscattered electron images obtained from the 2 ECAP passes sample. As indicated by the arrows, the DRXed grains are in dark contrast and the $Mg_{24}Y_5$ particles are shown in white contrast. The DRXed grains are mainly located around the deformed grains and secondary phases and formed the bimodal structure. The coarse deformed grains are elongated with a width of about 10-20 μm and a length less than 100 μm. The grain size of the DRXed grains, less than 1 μm, was measured from the TEM bright field images obtained from the 3 ECAP passes sample (Figure 4c). A high density of $Mg_{24}Y_5$ particles typically of 200 nm or smaller appear in the grain boundaries of the DRXed grains. The diffraction pattern (inset to Figure 4c) obtained from the particle is consistent with that expected from the $Mg_{24}Y_5$ of bcc structure. Figure 4d shows some LPSO lamellae which are occasionally observed in the DRXed grains. The LPSO phase, however, is not frequently observed in the DRXed grains.

The morphologies of the LPSO lamellae and the pre-existing $Mg_{24}Y_5$ phase after deformation are shown in Figure 5. The LPSO lamellae have kinked after 3 ECAP passes. The LPSO lamellae are zig-zag, with the kink boundaries appearing as straight dark lines (white arrow in Figure 5a). It is worth noting that the long $Mg_{24}Y_5$ phase (indicated by a black arrow) in the middle of the LPSO phase shows a similar kink morphology. When a kink forms in the LPSO lamellae, the surrounding thin matrix layers also deform in a similar manner. Figure 5b shows the pre-existing $Mg_{24}Y_5$ phase after ECAP. The large $Mg_{24}Y_5$ particles

5

were broken into smaller ones, but they are restrained by the surrounding LPSO lamellae which appear intact.

3.2 The SPT test

The load versus displacement curves obtained from the SPTs are shown in Figure 6. The SPT load-displacement curves of Mg-Zn-Y alloys display elastic bending (I), plastic bending (II), membrane stretching (III) and plastic instability (IV) as described in [21]. After 1 ECAP pass, the maximum load before failure increased significantly compared to that of the as-cast sample. With more ECAP passes, the maximum load increased further by small amounts. Although the yield strength cannot be obtained directly from the SPT load-displacement curve, it can be linked to the load at breakaway, which is the value measured at the end of the elastic domain [22]. Cheon and Kim [22] tested a SA508 pressure vessel steel and concluded that the yield stress is proportional to the load at breakaway with a coeffiecient which varies with the material and the thickness of the sample. After 1 ECAP pass, the load at breakaway increased from about 60 N to about 100 N. After 2 passes and 3 passes the load at breakaway further increased slightly. This indicates that the strength of the sample increased with each ECAP pass.

In the ECAP processed samples, a distinct load deflection, as illustrated by the arrow in Figure 6, can be observed after the linear elastic region. The load continues to increase after the load deflection, and then starts to drop when the displacement reaches about 0.5 mm. In order to understand the origins of the load deflection, a 2-pass ECAPed sample was tested using SPT and stopped right after the load deflection (Figure 7).

Figure 7a and 7b show that a long crack had appeared in the 2-ECAP pass sample stopped after the load deflected. The corresponding SPT load-displacement curve is shown in Figure 7c. The back-scattered electron image (Figure 7b) shows that the crack is parallel to the shear direction of the ECAP process (i.e. 45° from ED to LD). Figure 7d shows that near the centre of the crack contains a region decorated with a

6

large number of white small particles (see the magnified image) corresponding to the DRXed region associated with small $Mg_{24}Y_5$ particles. Figure 7e indicates some inclusions near the end of the crack. According to the EDS results (Figure 7f), the inclusions have high contents of Y, O and Mg, which probably came from the as-cast alloy.

As shown in the low magnification images (Figure 8), the fully developed cracks form a rosette pattern, in both the as-cast and the ECAP processed samples after SPT. This indicates that the crack was initiated at the centre of the specimen. The crack pattern on the as-cast sample is more symmetrical than in the ECAP processed samples which have large cracks in the center linked to secondary cracks father away. The higher magnification image obtained from the as-cast sample (Figure 9a) shows a cleavage fracture with numerous facets. After the ECAP processing, the fracture surface (Figure 9b) contains cleavage features as well as micro-voids. Figure 9c and 9d show higher magnification images of the DRXed region in the crack surface.

In addition, fracture information from the sample processed by 1-pass ECAP at 200 ℃ is also provided in Figure 10. The SEM image shows some cavities at low magnification and some straight traces (as indicated by the dashed lines) along the shear direction. At higher magnification, lots of voids and particles of about 100 nm in size are observed as shown in Figure 10b. The large number of voids on the fracture surface are often linked to the ductile failure. The morphology and size of the particles observed on the facture surface and those $Mg_{24}Y_5$ particles shown in Figure 4 are very alike.

3.3 Texture evolution during ECAP

EBSD results mainly obtained from the coarse deformed Mg grains are shown in Figure 11 which indicates that strong textures have formed after ECAP. The orientation map of the as-cast alloy is given in Figure 11a, which suggests that the grains in the as-cast condition have random orientations. After 1 ECAP pass, the texture intensity peak in the (0001) pole figure is found at 60° from ED towards LD. After 2 passes two peaks are found (at 77° and at 41°). After 3 passes, the basal plane is inclined at 45° to

7

the ED. In principle, the texture of hexagonal crystals after the first pass of ECAP should be a simple shear fibre at 45° from ED to LD; after 2 passes with the sample rotated by 90°, the symmetry of the (0001) texture component formed after the first pass of ECAP is lost [23]. Valle et al [24] reported that an AM60 alloy, after 2 ECAP passes, showed a simple shear fibre texture. In the current experiment, the (0001) pole figures show that the key texture components after $1 - 3$ passes of ECAP are all close to 45° from ED to LD.

The DRXed Mg grains are difficult to analyse using conventional EBSD due to their limited size and the presence of adjacent small $Mg_{24}Y_5$ particles. In order to characterise the texture of the DRXed grains, a thin foil of the 3-pass ECAP sample was studied using TKD. Figure 12a is a secondary electron image showing a deformed Mg grain surrounded by DRXed grains. The corresponding EDS maps (Figure 12b and 12c) show that Y is highly concentrated in some particles, and a slightly higher content of Zn element is also observed within the particles. These particles are indexed as $Mg_{24}Y_5$ in the phase map (yellow phase in Figure 12d). Using also the orientation map (Figure 12e), the $Mg_{24}Y_5$ particles lie on the grain boundaries of small Mg grains (upper-left and lower-right area), and are absent from the large deformed Mg grains (centre area where two large deformed Mg grains are found) which contain lots of subboundaries. The inverse pole figures of both phases are shown in Figure 12f. Besides the heavily deformed magnsium, the recrystallized Mg grains and $Mg_{24}Y_5$ particles are scattered across the whole area, and their is no obvious texture in the recrystallised region.

4. Discussion

The bimodal structure of the ECAP processed alloys and the cracks generated in the bimodal structure during SPT will be discussed in turn.

4.1 Bimodal structure

The grain size and texture of the Mg-Zn-Y alloys changed significantly after ECAP. The resultant microstructure after ECAP exhibits a bimodal grain size: coarse deformed grains (including Mg and LPSO) and fine DXRed Mg grains associated with small $Mg_{24}Y_5$ particles. In LPSO-free alloys, e.g. Mg-0.8%Al solid solution, Ion et al. [25] suggested that DRXed grains formed from the severely rotated regions adjacent to the original grain boundaries and that the original grain centre remain unchanged. In the current Mg-Zn-Y alloy containing LPSO and $Mg_{24}Y_5$ phases, the DRXed grains are mainly found around deformed Mg grains, which agrees with Ion et al [25]. However, with the presence of the second phases (especially LPSO), the DRXed grains and deformed grains also show some differences and will be discussed below.

First, the deformed grains were refined by kinking, where many kink boundaries were introduced into the LPSO and into the LPSO-associated Mg matrix. The LPSO phase is known to deform by kinking during processing [26]. Although limited activity of <a> type dislocations on prismatic planes has been observed during hot extrusion at 400 ℃ [27], the LPSO phase is highly anisotropic due to its ordered crystallographic structure and is hard to deform other than by <a> type basal slip, i.e. there are no <c+a> or <c> dislocations or twinning. Consequently, kinking is commonly observed when the LPSO phase is subjected to plastic deformation and sudden basal dislocation avalanches occur within a localised deformation zone. It is interesting to notice from the current work (Figure 5) that kinking is frequently observed in the magnesium matrix containing lamellar LPSO phase (sandwich structure of Mg/LPSO), and occasionally exists in the $Mg_{24}Y_5$ (Figure 5) as well, although the mechanism causing the Mg matrix and $Mg_{24}Y_5$ to kink may be different from that for kinking in the LPSO phase. For example, Shao et al. [8] observed that prismatic slip caused a Mg slice to shear along the kink direction. Generally, the thin Mg slice is surrounded by the LPSO phase, especially when the density of LPSO is high. Lamellar LPSO phase exists widely in the matrix, which makes kinking frequent in the current deformed alloy.

Unlike the LPSO phase, the pre-existing $Mg_{24}Y_5$ is a complex metallic alloy, just like $Mg_{17}Al_{12}$, shows extreme brittleness at room temperature [28]. The existence of large intermetallic particles is often

9

undesirable due to their brittleness and the likelihood of crack initiation. On the other hand, fine and well dispersed intermetallic particles are very effective strengthers. The large shear strains introduced by ECAP break up the micron-sized $Mg_{24}Y_5$ particles, but they are not effectively re-distributed because of the surrounding LPSO phase.

Secondly, the DRXed Mg grains are also found around large LPSO phase, although the largest number of DRXed grains is found around deformed Mg grains. The close linkage between DRX and LPSO phase has also been reported elsewhere [10, 29]. It was suggested that the LPSO phase can accelerate DRX through particle-stimulated recrystallisation [29]. Humphreys [30] proposed that if the particle is non-deformable then local plastic deformation must maintain the particle in its original shape, leaving the matrix sheared, and that DRX occurs in the deformed zone near the particles. However, the LPSO phase is deformable and is only a little harder than the Mg matrix [31]. The critical resolved shear stress (CRSS) of basal slip for a Mg-1.0Y single crystal is about 9.5 MPa [32], which is slightly higher than that of the LPSO phase (about 7 MPa) estimated using a single phase LPSO pillar compression [33], and lower than the 10-30 MPa estimated by compression of directionally solidified polycrystalline LPSO [26]. This is different from typical particle stimulated recrystallisation where the particles are typically non-deformable. However, although the LPSO phase is deformable, the fact that its plasticity is confined to basal slip suggests that it would not be possible to transfer any non-basal slip activity in the Mg matrix into the LPSO phase. Strain localisation in the vicinity of the LPSO is therefore expected and would also promote the DRX.

Accompanying the DRXed grains, small $Mg_{24}Y_5$ particles have formed. The concentration of Y in the Mg matrix is high, so the precipitation of $Mg_{24}Y_5$ particles might be assisted by the large shear strain imposed and therefore the high dislocation density caused by the ECAP process. For instance, the sub-grain boundaries in the deformed microstructures may act as heterogeneous nucleation sites for $Mg_{24}Y_5$ particles. This is also consistent with the observation that the $Mg_{24}Y_5$ particles observed always lie along the grain boundaries of the DRXed grains. The $Mg_{24}Y_5$ particles could effectively restrain grain growth

by inhibiting boundary migration. Such an effect could be estimated following the Zener-Smith equation $d_{crit} \approx 4r/3f$ [34], where d_{crit} is the critical grain diameter, r is the radius of the particle and f is the volume fraction of the particles. The critical grain size is about 1 μm, taking the volume fraction and radius of the $Mg_{24}Y_5$ particles to be about 16 % and 120 nm (estimated from TEM observations) in the DRXed regions. The measured average DRXed grain size is about 600 nm and the largest is around 1 μm. This agrees with the critical grain size. The SPT strength of the Mg-Zn-Y alloys increased significantly after ECAP, which comes as no surprise due to the reduced grain size.

4.2 SPT crack analysis

The crack morphology of the bimodal structure is quite different along the ECAP shear direction and the perpendicular direction. The initial crack, which was observed immediately after elastic deformation, lies in the direction parallel to the shear direction.

Figure 1 shows a schematic drawing of the ball and disc contact during the SPT. The sample disc is round with its edge supported by the die and the loading is applied though the spherical ball to the disc. The stresses on the disk are symmetrical along the radial directions. As shown in Figure 7 and Figure 8, the crack starts in the central region of the bottom surface. Byun et al. [35] described the stress states at the centre of the bottom surface and indicated that the principal stress component along the z direction, σ_{zz}, is zero as the bottom surface is free of contact. The stress state is biaxial and the two perpendicular principal stress components along x and y directions, σ_{xx} and σ_{yy}, are equal and always tensile. The 3D stress state at the bottom centre is also shown in Figure 13a. Figure 13b shows a schematic drawing of the bimodal structure of the ECAP processed alloy under the tensile stress. The deformed coarse grains show a fibre texture according to the EBSD data, where the c direction is indicated in the figure. The DRXed Mg grains (coloured ones) show random orientations mainly located in the interior of the coarse deformed grains.

11

When the tensile stress applied on the bimodal structure increased, the large Mg grains, LPSO phase and DRXed grains started to deform at different stress levels. The deformation sequence of the $Mg_{97}Zn_1Y_2$ alloy with bimodal structure has been investigated by Garces et al. [13], which suggested that the coarse Mg grains deform when the stress is below the macroscopic yield stress, followed by the fine Mg grains above the macroscopic yield strength with the coarse LPSO grains remaining elastic. The Mg matrix deformation is dominated by twinning and basal slip. However, in the present study, no twinning has been observed during ECAP. In fact, kinking was frequently observed in the Mg matrix associated with the abundant LPSO phase. As indicated in Figure 13b, the deformed large grains show a preferential fibre texture, with the basal plane being parallel to the shear direction. The dominant basal slip of the deformed Mg and LPSO in the shear direction and its perpendicular direction is suppressed by the low Schmid factor, close to zero. Prismatic slip, pyramidal slip and twinning are limited by the small spacing between the LPSO lamellae in the Mg matrix. So deformation of the large Mg grains is unlikely in both directions. Compared with the large Mg grains, the macroscopic yield stress of the DRXed grains is normally higher due to the presence of the grain boundaries. In this case, the DRXed grains have random orientations and include many grains with high Schmid factors which started plastic deform first. The DRXed grains can only accommodate limited strain. With increasing stress, the DRXed grains could not longer accommodate the imposed strain and cracks start to form. In the bimodal structure DRXed grains exhibit thin layers between the deformed Mg grains, almost parallel to the shear plane and continuously across the whole sample. Once the crack has formed in the DRXed grain region, it will grow easily along the shear direction since there is a perpendicular tensile stress component. This leads to a less symmetrical morphology of the fully developed cracks in the ECAP processed alloys compared that of the as-cast alloy. Yamasaki et al. [10] reported that the DRXed grains increased the ductility of the extruded $Mg_{97}Zn_1Y_2$ alloys, which seems contradictory to the current result that the DRXed grains act as potential crack sites during SPTs. It needs to be clarified that Yamasaki et al. [10] focused on the ductility changes caused by different area fractions of DRXed grains in the extrusion direction, while this work focused on comparing the ductility differences of the bimodal structure in different directions and the direct evidence

of the ductility changes after ECAP is not provided. The DRXed grains accommodate the initial deformation in both directions and become potential crack sites during further deformation. When the tensile stress is applied to the shear direction, the crack can be hindered by the coarse Mg and LPSO grains. But when the tensile stress is applied to the perpendicular direction, the cracks can grow freely along these DRXed grains. This indicates the effect of DRXed grains on the ductility may be different in the shear direction than in the perpendicular direction.

5. Conclusions

Mg-Zn-Y alloys after ECAP developed a bimodal structure with large elongated grains and small DRXed grains. LPSO phase tends to kink to accommodate the strain, introducing many kink boundaries into the surrounding matrix material. The LPSO phase also promotes DRX of the Mg matrix, while the fine $Mg_{24}Y_5$ particles located along the DRXed grain boundaries limit the grain growth. The SPT strength of the $Mg_{94}Zn_2Y_4$ alloy increased significantly after ECAP.

The bimodal structure exhibits asymmetrically shaped cracks along the ECAP shear direction and the perpendicular direction after SPT. The cracks start shortly after the linear elastic region during SPT under a biaxial tensile stress. The initial crack lies in the shear direction and DRXed grains are potential crack sources. This may be due to the strong fibre texture of the large grains with the presence of LPSO phase inhibiting the dominant basal slip and leading to the deformation first of DRXed grains. These observations show that the bimodal structure exhibits better ductility when the tensile stress is applied along the shear direction than the perpendicular direction. If ECAP is to be used to refine the microstructure of Mg-Zn-Y alloys and allows them to be employed as sheets it will be necessary to take into consideration the different deformation behaviours of the bimodal structure along different directions.

Acknowledgement

References

[1] Y. Kawamura, K. Hayashi, A. Inoue, T. Masumoto, Mater. Trans. 42 (2001) 1172-1176

[2] A. Inoue, Y. Kawamura, M. Matsushita, K. Hayashi, J. Koike, J. Mater. Res. 16 (2001) 1894-1900.

[3] Y. Kawamura, M. Yamasaki, Mater. Trans. 48 (2007) 2986-2992.

[4] K. Kishida, K. Nagai, A. Matsumoto, A. Yasuhara, H. Inui, Acta Mater. 99 (2015) 228-239.

[5] F. Lu, A. Ma, J. Jiang, D. Yang, Q. Zhou, Rare Metals 31 (2012) 303-310.

[6] M. Yamasaki, K. Hagihara, S.-i. Inoue, J.P. Hadorn, Y. Kawamura, Acta Mater. 61 (2013) 2065-2076.

[7] H. Liu, F. Xue, J. Bai, J. Zhou, Y. Sun, J. Mater. Sci. Technol. 30 (2014) 128-133.

[8] X.H. Shao, Z.Q. Yang, X.L. Ma, Acta Mater. 58 (2010) 4760-4771.

[9] J.-K. Kim, S. Sandlöbes, D. Raabe, Acta Mater. 82 (2015) 414-423.

[10] M. Yamasaki, K. Hashimoto, K. Hagihara, Y. Kawamura, Acta Mater. 59 (2011) 3646-3658.

[11] T. Itoi, T. Inazawa, M. Yamasaki, Y. Kawamura, M. Hirohashi, Mater. Sci. Eng. A 560 (2013) 216-223.

[12] G. Garces, M.A. Muñoz-Morris, D.G. Morris, P. Perez, P. Adeva, Mater. Sci. Eng. A 614 (2014) 96-105.

[13] G. Garces, D.G. Morris, M.A. Muñoz-Morris, P. Perez, D. Tolnai, C. Mendis, A. Stark, H.K. Lim, S. Kim, N. Shell, P. Adeva, Acta Mater. 94 (2015) 78-86.

[14] J.-M. Baik, J. Kameda, O. Buck, Scr. Metall. 17 (1983) 1443-1447.

[15] X. Mao, M. Saito, H. Takahashi, Scr. Metall. Mater. 25 (1991) 2481-2485.

[16] J.S. Ha, E. Fleury, Int. J. Pres. Ves. Pip. 75 (1998) 707-713.

[17] R.Z. Valiev, T.G. Langdon, Prog. Mater. Sci. 51 (2006) 881-981.

[18] P.W. Trimby, Ultramicroscopy 120 (2012) 16-24.

[19] D. Egusa, E. Abe, Acta Mater. 60 (2012) 166-178.

[20] Y.M. Zhu, A.J. Morton, J.F. Nie, Acta Mater. 60 (2012) 6562-6572.

[21] J.-M. Baik, J. Kameda, O. Buck, ASTM STP, 888 (1986) 92-111.

[22] J.S. Cheon, I.S. Kim, J. Test. Eval. 24 (1996) 255-262.

[23] I.J. Beyerlein, L.S. Tóth, Prog. Mater. Sci. 54 (2009) 427-510.

[24] J.A. del Valle, F. Carreño, O.A. Ruano, Acta Mater. 54 (2006) 4247-4259.

[25] S.E. Ion, F.J. Humphreys, S.H. White, Acta Metall. 30 (1982) 1909-1919.

[26] K. Hagihara, N. Yokotani, Y. Umakoshi, Intermetallics 18 (2010) 267-276.

[27] K. Hagihara, Y. Fukusumi, M. Yamasaki, T. Nakano, Y. Kawamura, Mater. Trans. 54 (2013) 693-697.

[28] J. Ragani, P. Donnadieu, C. Tassin, J.J. Blandin, Scr. Mater. 65 (2011) 253-256.

[29] L.B. Tong, X. Li, D.P. Zhang, L.R. Cheng, J. Meng, H.J. Zhang, Mater. Charact. 92 (2014) 77-83.

[30] F.J. Humphreys, Acta Metall. 25 (1977) 1323-1344.

[31] E. Oñorbe, G. Garcés, P. Pérez, S. Cabezas, M. Klaus, C. Genzel, E. Frutos, P. Adeva, Scr. Mater. 65 (2011) 719-722.

[32] S. Miura, S. Imagawa, T. Toyoda, K. Ohkubo, T. Mohri, Mater. Trans. 49 (2008) 952-956.

[33] A. Inoue, K. Kishida, H. Inui, K. Hagihara, Mater. Res. Soc. Symp. Proc. 1516 (2013) 151-156.

[34] C.S. Zener. Quoted by C.S. Smith, Trans. Met. Soc. AIME, 175 (1948) 15.

[35] T.S. Byun, E.H. Lee, J.D. Hunn, K. Farrell, L.K. Mansur, J Nucl Mater, 294 (2001) 256-266.

Figure captions:

Figure 1 Schematic drawing of the small punch test.

Figure 2 (a) Backscattered electron image obtained from the as-cast $Mg_{94}Zn_2Y_4$ alloy; (b) TEM bright-field image showing the LPSO and adjacent $Mg_{24}Y_5$; (c) Selected area diffraction pattern obtained from the LPSO phase showing it has the 18R type structure; the electron beam direction is parallel to the [1210] zone axis; (d) Selected area diffraction pattern obtained from $Mg_{24}Y_5$; the electron beam direction is parallel to the [111] zone axis.

Figure 3 Optical images obtained from the $Mg_{94}Zn_2Y_4$ alloy under the as-cast condition (a) and ECAP processed for 1-pass (b), 2-passes (c) and 3-passes (d), respectively.

Figure 4 Backscattered electron image showing at low magnification (a) and high magnification (b) a region of DRXed grains in the 2-pass ECAP processed $Mg_{94}Zn_2Y_4$ sample; (c) TEM bright field image showing DRXed grains together with some $Mg_{24}Y_5$ particles in a 3-pass ECAP processed sample; a diffraction pattern along [111] zone axis obtained from the arrowed $Mg_{24}Y_5$ particle is inset; (d) TEM bright field image showing the occasionally observed LPSO phase in a DRXed grain in the 3-pass ECAPed sample.

Figure 5 SEM backscattered electron image of a 3-pass ECAP processed sample: (a) showing the kinked microstructure of the LPSO phase: the white arrows represent the kink boundaries; (b) showing pre-existing $Mg_{24}Y_5$ fractured during ECAP

Figure 6 Load vs displacement curves obtained from the SPTs of the as-cast and ECAP processed samples.

Figure 7 (a) Secondary electron image and (b) Backscattered electron image of 2-pass sample showing crack initiated during SPT; (c) Corresponding SPT load-displacement curve showing how the test was stopped when a load deflection was observed after elastic deformation (see arrow); (d) Magnified images showing that the crack goes through the DRXed region; (e) Inclusions in the crack; (f) EDS spectrum of the inclusions which have a high content of Y, O and Mg.

Figure 8 Low magnification secondary electron images showing a crack in the SPT sample: (a) as-cast sample; (b) 1ECAP pass sample; (c) 2 ECAP passes sample; (d) 3 ECAP passes sample.

16

Figure 9 Images of fracture morphology in Mg-Zn-Y alloy after SPT: secondary electron images of (a) as-cast condition; (b) 2-pass sample; (c, d) secondary and backscattered electron images of the same area in the 2-pass processed sample.
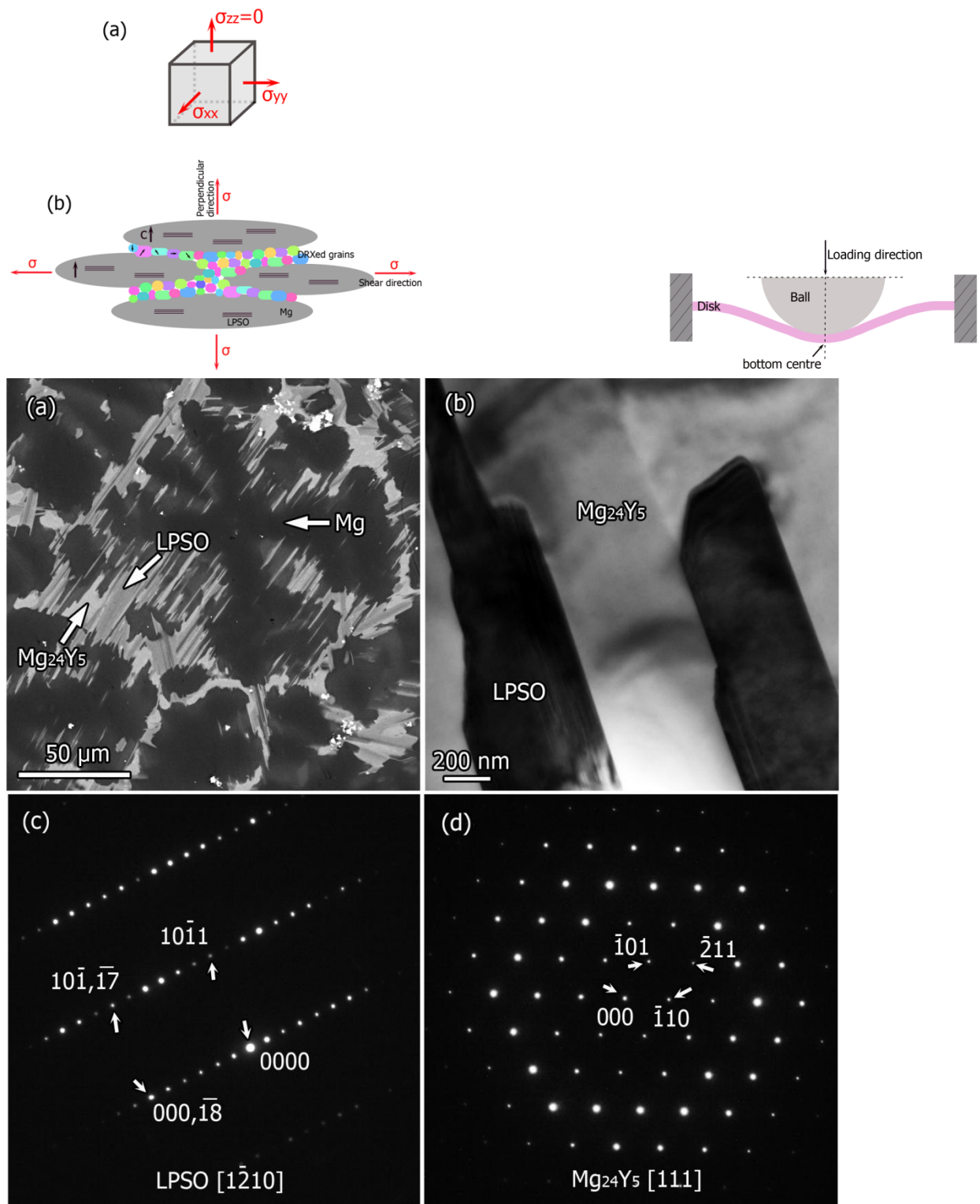
Figure 10 SEM images of fracture surface of the sample processed by 1-pass ECAP at 200 ℃: (a) lower magnification image shows a relatively flat surface; (b) higher magnification image shows a large density of voids and $Mg_{24}Y_5$ particles.
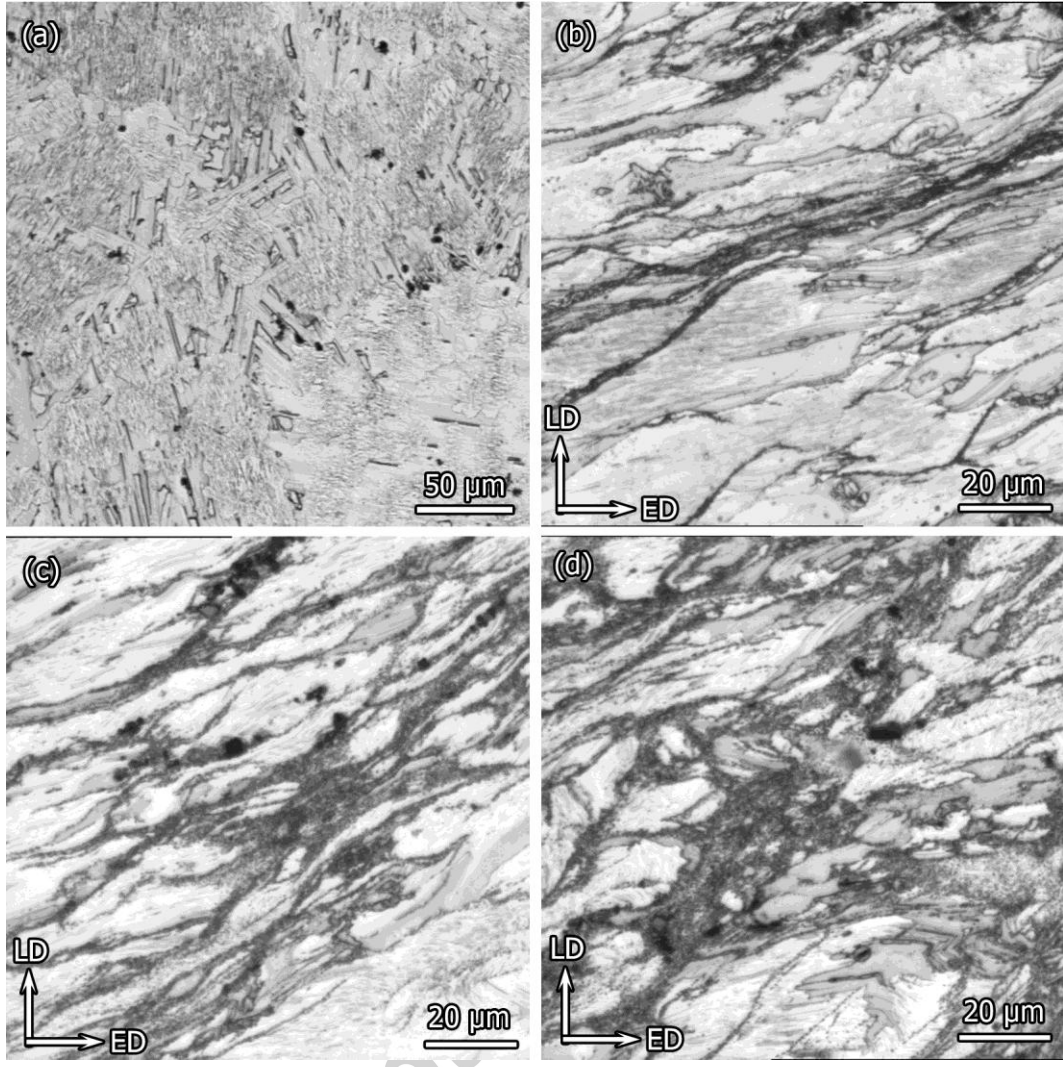
Figure 11 EBSD results obtained from the as-cast and ECAP processed samples: (a-d) IPF colour images of as-cast, 1-pass, 2-pass and 3-pass ECAP samples respectively; (e-h) Mg (0001) pole figures of the as-cast, 1-pass, 2-pass and 3-pass ECAP samples. The interval of the contour lines is 2, and the maximum intensity is indicated by an arrow.

Figure 12 TKD results from 3-pass ECAP sample: a) Secondary electron image of an typical area; b) EDS map for Y; c) EDS map for Zn; d) TKD phase map, with Mg as red, $Mg_{24}Y_5$ as yellow and zero solution spots as white; (e) Orientation map; (f) inverse pole figures of Mg and $Mg_{24}Y_5$.

Figure 13 (a) The 3D stress state at the bottom centre of the disk; (b) The biaxial stress state of the bimodal structure at the bottom centre.
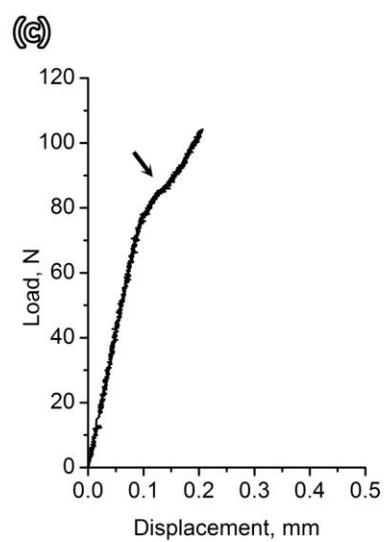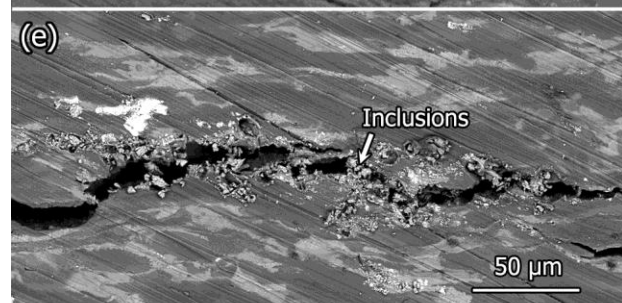
FIGURES

(a)

$\sigma_{zz}=0$

σ_{yy}

σ_{xx}

(b)

Perpendicular direction σ

c

σ

DRXed grains

σ

Shear direction

LPSO

Mg

σ

Loading direction

Disk

Ball

bottom centre

(a)

Mg

LPSO

Mg₂₄Y₅

50 μm

(b)

Mg₂₄Y₅

LPSO

200 nm

(c)

10$\bar{1}$1

10$\bar{1}$,$\bar{1}$7

0000

000,$\bar{1}$8

LPSO [1$\bar{2}$10]

(d)

$\bar{1}$01

$\bar{2}$11

000

$\bar{1}$10

Mg₂₄Y₅ [111]